THE ASTRONOMICAL JOURNAL, 120:1325–1341, 2000 September

HUBBLE SPACE TELESCOPE IMAGING OF THE CIRCINUS GALAXY[1]

A. S. WILSON
Space Telescope Science Institute, 3700 San Martin Drive, Baltimore, MD 21218; awilson@stsci.edu; and Astronomy Department, University of Maryland, College Park, MD 20742; wilson@astro.umd.edu

P. L. SHOPBELL[2]
Astronomy Department, University of Maryland, College Park, MD 20742; pls@astro.umd.edu

CHRIS SIMPSON
Subaru Telescope, National Astronomical Observatory of Japan, 650 North A'ohuku Place, Hilo, HI 96720; chris@naoj.org

T. STORCHI-BERGMANN AND F. K. B. BARBOSA
Instituto di Fisica, Universidad Federal do Rio Grande do Sul, Porto Alegre, RS 91501-970, Brazil; thaisa@if.ufrgs.br

AND

M. J. WARD
Department of Physics and Astronomy, University of Leicester, University Road, Leicester, LE1 7RH, England, UK; mjw@star.le.ac.uk
Received 2000 May 8; accepted 2000 June 8

ABSTRACT

We present a *Hubble Space Telescope* imaging study of the nearby (4 Mpc distant) Circinus galaxy, which contains the nearest type 2 Seyfert nucleus and prominent circumnuclear star formation. Images have been obtained in the [O III] λ5007, Hα, and H_2 $v = 1$–0 $S(1)$ emission lines, and in the green (5470 Å), red (8140 Å), and near-infrared (2.04 and 2.15 μm) continua. An image in the [Fe II] λ1.644 μm line has been taken with a ground-based telescope. The [O III] and Hα images reveal the detailed structure of the complex of streamers and knots of high-excitation gas, which extends out of the galaxy disk. The morphology some 250 pc from the nucleus strongly suggests that the high-excitation gas is concentrated on the surface of a hollow cone with apex close to the nucleus. Such a structure may result through entrainment of dense gas from a circumnuclear torus in the galaxy disk by a low-density, outflowing wind or jet. Within 40 pc of the nucleus, the high-excitation gas takes the form of a striking, filled V-shaped structure extending in the same direction as the larger scale high-excitation emission. This V can be described as an ionization cone, though a matter-bounded structure is also possible. The implied collimation of the ionizing photons or gaseous outflow must occur within 2 pc of the apex of the cone, presumed to be the location of the nucleus.

The Hα image shows a complex structure of H II regions, including the well-known starburst ring of radius 150–270 pc. In addition, there is a more compact (40 pc radius), elliptical ring of H II regions around the ionization cone. We argue that this latter ring, which we call the nuclear ring, is intrinsically circular and located in the plane of the galaxy disk. Much of the [Fe II] emission is associated with this nuclear, star-forming ring and is presumably powered by supernova remnants. Hot molecular hydrogen extends to within 10 pc of the nucleus, and possibly closer. The intrinsic infrared–optical continuum colors in the inner regions of the Circinus galaxy are, in many locations, bluer than is typical of bulges, indicating a relatively young stellar population is present. We confirm the presence of a compact (<2 pc), very red nuclear source in the K band. Its properties are consistent with a type 1 Seyfert nucleus viewed through an obscuration of $A_V = 28 \pm 7$ mag.

Key words: galaxies: active — galaxies: individual (Circinus) — galaxies: ISM — galaxies: nuclei — galaxies: Seyfert — galaxies: starburst

1. INTRODUCTION

The Circinus galaxy is a large, highly inclined ($i = 65°$), spiral galaxy of uncertain morphological type seen through a Galactic window with low extinction ($A_V = 1.5 \pm 0.15$ mag) at $b = -4°$ (Freeman et al. 1977). It contains both a type 2 Seyfert nucleus and a circumnuclear starburst and, in view of its proximity (distance 4 ± 1 Mpc, thus $1'' = 19$ pc), has been intensively studied in recent years. The Seyfert activity was first found through the discovery of water vapor megamaser emission (Gardner & Whiteoak 1982), a phenomenon apparently associated exclusively with Seyfert or LINER-type active nuclei (Braatz, Wilson, & Henkel 1997). Individual water vapor maser spikes vary on timescales as short as a few minutes (Greenhill et al. 1997), and the masing gas traces a thin accretion disk about 0.8 pc in radius with, in addition, a significant population of masers that lie away from the disk and may be in outflow (Greenhill et al. 1998). The X-ray spectrum below 10 keV exhibits a flat continuum and a very prominent iron line, indicative of Compton scattering and fluorescent emission from gas illuminated by an obscured X-ray continuum source (Matt et al. 1996). Recent observations above 10 keV have revealed excess emission above an extrapolation of the 0.1–10 keV spectrum suggesting that, at the higher energies, the nucleus is seen directly through a column density of $\sim 4 \times 10^{24}$ cm^{-2} (Matt et al. 1999). Optical and near-

[1] Based on observations with the NASA/ESA *Hubble Space Telescope* obtained at the Space Telescope Science Institute, which is operated by the Association of Universities for Research in Astronomy, Inc., under NASA contract NAS 5-26555.

[2] Present address: Department of Astronomy, Mail Code 105-24, California Institute of Technology, Pasadena, CA 91125; pls@phobos.caltech.edu.

infrared spectrophotometry of the nucleus show a typical Seyfert spectrum, including strong coronal lines (Oliva et al. 1994; Maiolino et al. 1998). Emission lines from highly ionized species are also found in a 2.5–45 μm spectrum obtained with the *Infrared Space Observatory* (*ISO*) (Moorwood et al. 1996). The gas is generally believed to be photoionized though quite different photoionization models (Moorwood et al. 1996; Binette et al. 1997; Oliva, Marconi, & Moorwood 1999) can reproduce the observed emission-line ratios. Optical spectropolarimetry reveals polarized and relatively broad (FWHM ~ 3300 km s^{-1}) Hα emission from a region less than 60 pc in extent centered on the nucleus, indicating the presence of a "hidden" broad-line region (Oliva et al. 1998).

Highly ionized gas extends along the minor axis of the galaxy, with a morphology that widens with increasing distance from the nucleus and is reminiscent of the so-called ionization cones seen in some Seyfert galaxies (Marconi et al. 1994). The cone in Circinus does not, however, show the filled structure with sharp, straight edges seen in some other Seyfert galaxies (e.g., NGC 5728; Wilson et al. 1993) and that strongly suggests the gas is ionized by a shadowed nuclear UV source. A complex of ionized filaments is found within the cone and extending radially from the nucleus out to distances of 1 kpc, as well as arcs suggestive of bow shocks at the termini of some of these filaments (Veilleux & Bland-Hawthorn 1997; Elmouttie et al. 1998b). The filamentary gas appears to be flowing outward from the nucleus at velocities of 200 km s^{-1} or higher. In the radio continuum (Elmouttie et al. 1995, 1998a), there is a compact (<20 pc diameter) flat spectrum nuclear source plus an extended crosslike structure. One arm of the cross extends along the galaxy disk and is believed related to star formation activity, while the other extends orthogonal to it. The orthogonal radio features are strongly polarized and comprise a bisymmetric plume and edge-brightened lobes.

A circumnuclear star-forming ring of diameter $\simeq 200$ pc is delineated by H II regions and seen clearly in Hα images (Marconi et al. 1994; Elmouttie et al. 1998b). There is also a molecular disk (Elmouttie et al. 1998c) or ring (Curran et al. 1998) of radius ~ 300 pc, which presumably provides the gas for the star formation. *ISO* spectra show polycyclic aromatic hydrocarbon features between 5 and 12 μm that are remarkably similar to those found in "pure" starburst spectra. There are also lines from H_2 and low-excitation ionic species, both believed to be associated with star-forming regions (Moorwood et al. 1996). The distribution and kinematics of the H_2 $v = 1$–0 $S(1)$ line have been studied from the ground via imaging (Maiolino et al. 1998; Davies et al. 1998) and long-slit spectroscopy (Storchi-Bergmann et al. 1999). High-resolution Brγ imaging (Maiolino et al. 1998) has been interpreted in terms of ongoing star formation activity within a few tens of parsecs of the active nucleus. Maiolino et al. (1998) find that, between the 100 pc and 10 pc scales, the stellar population is relatively young with an age between 4×10^7 and 1.5×10^8 yr. They argue that the starburst may have propagated outward from the nucleus to the 200 pc diameter ring, where hot young stars are currently forming. The luminosity of the starburst within a 200 pc radius is $\simeq 1.7 \times 10^{10}\ L_\odot$ (Maiolino et al. 1998), while the luminosity of the Seyfert nucleus is comparable at $\sim 10^{10}\ L_\odot$ (Moorwood et al. 1996). Together, the two contribute most of the luminosity of the galaxy (Maiolino et al. 1998).

The proximity of this Seyfert plus circumnuclear starburst galaxy invites further study. The connection between nuclear activity and circumnuclear star formation is a topic of great current interest (e.g., Cid Fernandes & Terlevich 1995; Genzel et al. 1995; Storchi-Bergmann et al. 1996; Heckman et al. 1997; González Delgado et al. 1998) but can be probed only by high spatial resolution observations. High spatial resolution imaging is also needed to investigate the origin and nature of the gaseous outflow within the "ionization cone." Such observations can also potentially investigate the morphology of the gas and dust responsible for the obscuration of the nucleus in type 2 Seyfert galaxies.

In this paper, we report an optical and near-infrared imaging study of the Circinus galaxy with the *Hubble Space Telescope* (*HST*), which provides a resolution better than 0.″1 (2 pc) at optical wavelengths. We have obtained images in the gaseous emission lines [O III] λ5007, Hα, and H_2 $v = 1$–0 $S(1)$ at 2.12 μm, and in the green (5470 Å), red (8140 Å), and near-infrared (2.04 and 2.15 μm) continua. In addition, we have obtained an image in the [Fe II] λ1.644 μm line with a ground-based telescope.

2. OBSERVATIONS AND REDUCTION

2.1. *HST Optical Observations*

As part of GO program 7273, the Circinus galaxy was observed by *HST* with the WFPC2 instrument on 1999 April 10. This target lies at the heart of the southern continuous viewing zone (CVZ), allowing us to obtain 3500 s of exposure in a single orbit. The galaxy was centered on the PC chip, in order to obtain the maximum spatial resolution on the nucleus and ionization cone regions. Images were obtained through filters isolating the emission lines of [O III] λ5007 (F502N) and Hα (F656N), as well as corresponding green and red continuum regions (filters F547M and F814W). The exposure times were 2×900 s and 2×800 s for the [O III] and Hα imagery, respectively. No anomalies were reported during the observation period.

The data were reduced in the standard fashion, using the IRAF/STSDAS software package.[3] Although the data were received in calibrated form, they were recalibrated and reduced in order to take advantage of more up-to-date calibration reference files. This procedure was accomplished by the CALWP2 task, which removes the CCD bias level, subtracts the dark current component, and flat-fields the pixel-to-pixel response of the chips. Cosmic rays were removed by combining two images in each of the separate filters, using the anticorrelation technique implemented in the CRREJECT task. The images were carefully surveyed by hand and additional cosmic rays identified and removed by interpolation.

The data were flux-calibrated using the SYNPHOT package for synthetic photometry, together with the most recent *HST* filter and telescope throughput tables. A corresponding continuum image was constructed for each narrowband image by assuming a linear continuum and interpolating from the broadband images. The alignment of the images was then verified using a number of stars in the fields; small offsets were applied. The continuum was subtracted from each of the narrowband images to derive maps

[3] IRAF is distributed by the National Optical Astronomy Observatories, which are operated by the Association of Universities for Research in Astronomy, Inc., under cooperative agreement with the National Science Foundation.

of the Hα and [O III] line flux. We produced maps encompassing the entire 160″ field of the WFPC2 instrument (0.″1 pixel^{-1}), as well as the 36″ field of the high-resolution PC chip (0.″046 pixel^{-1}).

We have also produced a map of the line ratio [O III]/Hα and of the continuum color $V-I$. Each of the [O III] and Hα images was "clipped" at a signal-to-noise (S/N) ratio of 1. The line ratio map was calculated at all points where *either* map has S/N > 1. Because Hα is seen from all gas that emits [O III], but [O III] is detected from only the high-excitation gas, our procedure implies that the calculated ratio is an actual measurement only where [O III] is detected, and an upper limit elsewhere (in H II regions ionized by hot stars, for example).

The F656N filter has a peak transmission at 6561 Å and a width $\delta\lambda = 21.4$ Å (as defined in the WFPC2 Instrument Handbook). At the heliocentric systemic velocity of Circinus (439 ± 2 km s^{-1}; Freeman et al. 1977), both [N II] λ6548 and Hα fall on the flat part of maximal transmission in the filter profile. Because there is very little gas with recession velocity below 100 km s^{-1} (see Fig. 4 of Elmouttie et al. 1998b), the contribution of [N II] λ6583 to our F656N image is always negligible. In H II regions F([N II] λ6548) $\ll F$(Hα), and so [N II] is a negligible contributor to the image in these regions. There will be some contribution from [N II] λ6548 in the high-excitation gas; this contribution is difficult to quantify in view of the spatial variation of recession velocity and the minimal number of published measurements of the spatial dependence of F([N II] λ6548)/F(Hα). With this caveat, we shall refer to the continuum-subtracted F656N image as "Hα."

2.2. *HST Infrared Observations*

An additional four CVZ orbits were used to observe the Circinus galaxy with the NICMOS Camera 2 through filters F204M, F212N [on-band H_2 $v = 1$–0 $S(1)$], and F215N (off-band H_2). A total of 6656 s was spent on the galaxy in each of the narrowband filters, using five different dither positions. These were bracketed by two 128 s on-source observations in the F204M filter, both taken at the same position. At the time of designing the NICMOS observations, the temporal stability of the thermal background was not known. Therefore, three regions of sky located approximately 10′ from the center of the galaxy were also observed to facilitate background subtraction; observations of 512 s each in the F212N and F215N filters were made at the start, middle, and end of the visit, and observations of 256 s with the F204M filter were made at the start and end of the visit.

The first step in the data reduction was to perform a subtraction of the NICMOS "pedestal" using software written and kindly provided by R. van der Marel. A study of the background images revealed no significant variations in either structure or count rate, and these were therefore combined, using median filtering to remove Galactic stars, to produce a single background image for each filter.

The images taken at each dither position in the F212N and F215N filters were stacked and background-subtracted. They were then combined using the CALNICB task with integer pixel shifts determined from centroiding of the bright nucleus. The two F204M images were similarly combined, although no shift was necessary.

As a final step, an image of the H_2 $v = 1$–0 $S(1)$ emission line only was constructed by subtracting an estimated continuum level from the F212N line-plus-continuum image. Several combinations of the F204M and F215N (which possessed similar signal-to-noise ratios) were investigated, with there being no significant differences between the results. We therefore chose to construct a continuum image at the pivot wavelength of the F212N filter by assuming that the continuum S_λ was a linear function of λ between the F204M and F215N filters.

2.3. *Ground-based Infrared Observations*

Infrared images of Circinus were obtained through an H-band filter and a narrowband [Fe II] λ1.644 μm filter using the CIRIM imager at the 4 m Blanco telescope at CTIO on the night of 1999 May 25. The total integration times were 180 s for the H-band and 1800 s for the narrowband observation, which was split into nine individual exposures. Sky frames were obtained at 10′ from the galaxy. The scale was 0.″21 pixel^{-1}, and the seeing was ≈0.″9.

Reduction of the ground-based images followed standard procedures in IRAF. The images were corrected for extinction using average coefficients for Cerro Tololo (Frogel 1998). Because the weather became cloudy before a standard star could be observed, flux calibration of the H- and narrowband images was performed using the aperture photometry of Moorwood & Glass (1984). We have adopted the H-band image as the continuum (off-band) for the [Fe II] λ1.644 μm image because the bad weather precluded obtaining a continuum image through a narrower filter. Two potential problems must be considered when adopting this procedure. First, the H filter contains the [Fe II] λ1.644 μm line. From Storchi-Bergmann et al. (1999), we estimate that the equivalent width of the [Fe II] λ1.257 μm line (which has comparable flux to the 1.644 μm line—[Fe II] λ1.644 μm/1.257 μm = 0.74—Nussbaumer & Storey 1988) is $\lesssim$5 Å, much less than the FWHM ≈ 3300 Å of the H-band filter, and so the contribution of the [Fe II] emission to the H-band image is negligible. Second, the H filter is much wider than the [Fe II] filter. However, it is approximately centered on the line, so differences in continuum level due to color variations should be small.

The continuum-subtracted [Fe II] image was obtained by scaling the narrowband image with respect to the H-band image. We first tried using the scale factor obtained from the ratio between the integrated counts of a field star in the H image and in the [Fe II] image (only one star in our images was bright enough for this purpose). The resulting subtracted image was negative around the nucleus, indicating that color effects were present and that we had oversubtracted the galaxy continuum. We then progressively increased the scale factor used to multiply the [Fe II] image until the negative counts were eliminated. This was obtained by a 12% increase of the factor obtained from the stellar counts.

3. RESULTS

3.1. *Optical Images*

The *HST* optical images obtained with WFPC2 are shown in Figures 1, 2, 3, 4, and 5. The orientation is such that the major axis of the galaxy (PA $30^\circ \pm 5^\circ$; Freeman et al. 1977) runs horizontally and the near side (southeast) of the galaxy disk is in the lower part of the panels.

Figure 1 shows the large-scale structure of the galaxy in Hα (*upper panel*) and in the I-band continuum (*lower panel*).

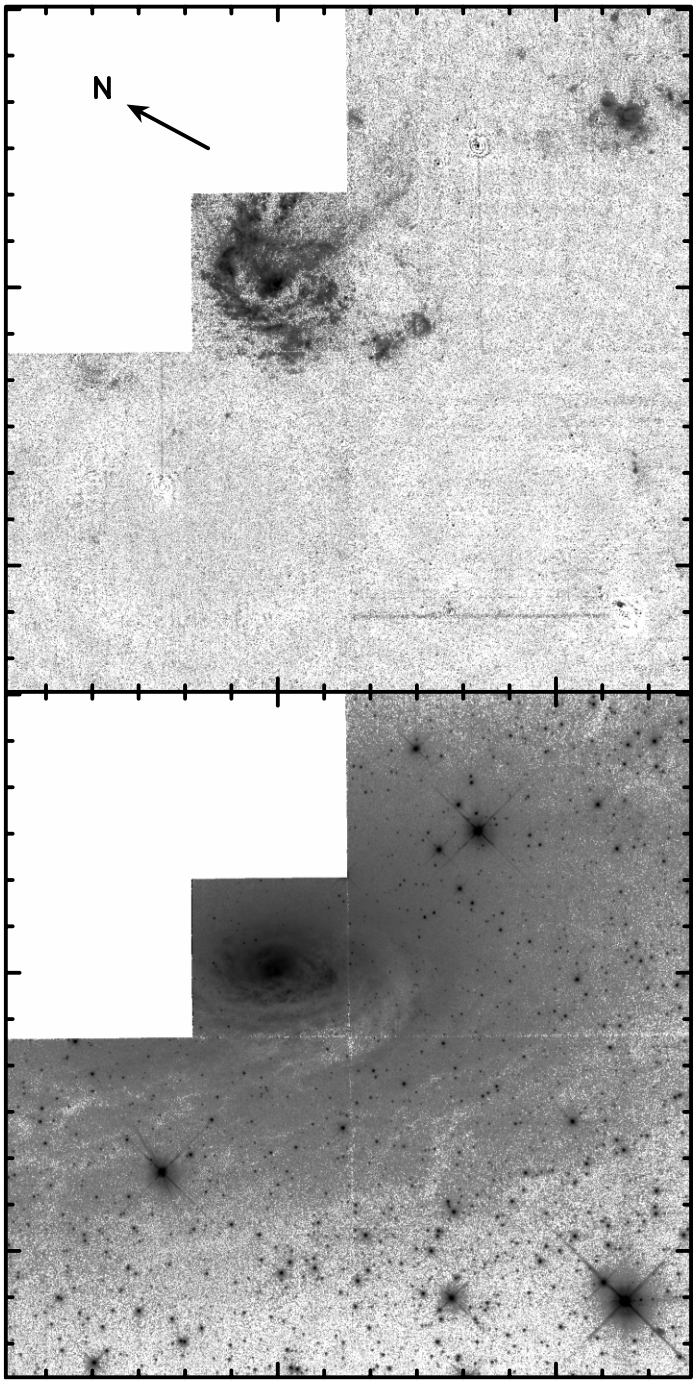

FIG. 1.—*HST* images of the Circinus galaxy, showing the whole field covered by the PC and WF camera chips. The image received on the PC chip has been binned to the WF pixel size of 0.″0996. Long tick marks are separated by 1′ and short tick marks by 10″. A long tick mark on each axis is aligned with the apex of the "ionization cone." The whole field of each panel is 148″ × 148″. The direction of north is rotated +61.°8 from the vertical and is indicated by the arrow. Darker shades represent brighter regions. The shading in both images is on a logarithmic scale. *Top*: Continuum-subtracted Hα image. The shading ranges between 3×10^{-18} (*white*) and 5×10^{-16} (*black*) ergs cm^{-2} s^{-1} $pixel^{-1}$. *Bottom*: Image through F814W filter (continuum). The shading ranges between 1×10^{-16} (*white*) and 2×10^{-14} (*black*) ergs cm^{-2} s^{-1} $pixel^{-1}$ in the filter band.

Some 1.′5 to the southwest of the nucleus (*upper right-hand portion of figure*) in the Hα image is a region of emission that is also apparent in the ground-based Hα imaging of Elmouttie et al. (1998b, their Fig. 1*a*). Elmouttie et al. note the coincidence of this feature with compact radio continuum emission and argue that it is an H II region. The absence of [O III] λ5007 at this location in our images supports this interpretation. Two diffuse patches of line emission, also apparently H II regions and visible in ground-based images (Marconi et al. 1994; Elmouttie et al. 1995), are found ≃30″ south of the nucleus. A linear feature, seen in ground-based [O III] λ5007 (Veilleux & Bland-Hawthorn 1997) and Hα + [N II] (Marconi et al. 1994) images, extends ≃40″ to the southwest of the nucleus, onto the upper right WF chip. This feature is not detected in our [O III] λ5007 image and is thus of lower excitation than the high-excitation gas (discussed below) to the northwest of the nucleus (cf. Fig. 6 of Marconi et al. 1994). The *I*-band image

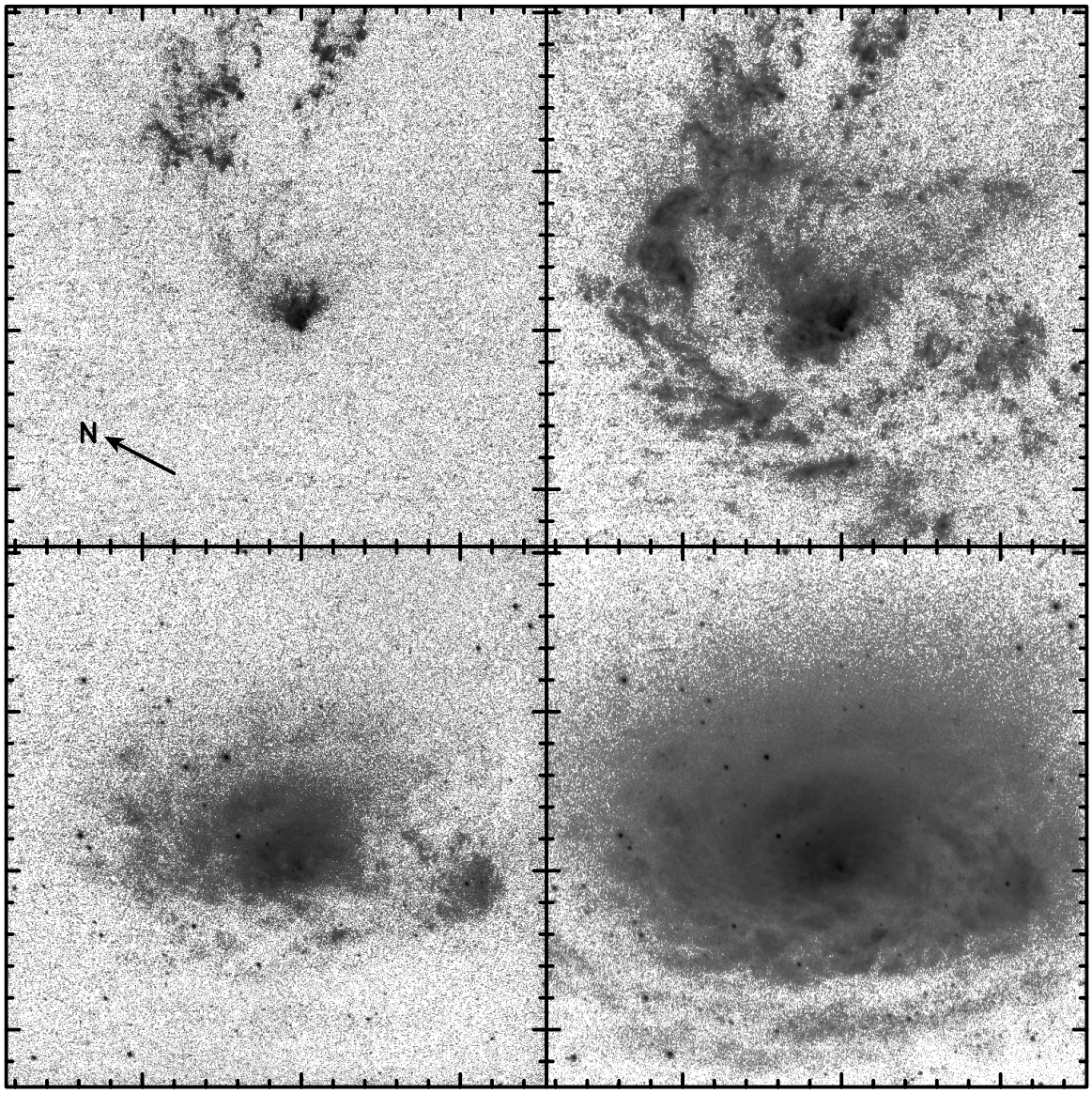

FIG. 2.—*HST* images of the Circinus galaxy, showing the PC chip only. The pixel size is 0.″0455. Long tick marks are separated by 10″ and short tick marks by 2″. A long tick mark on each axis is aligned with the apex of the "ionization cone." The field of each panel is 34.″0 × 34.″0. The direction of north is rotated +62.°2 from the vertical and is indicated by the arrow. Darker shades represent brighter regions. The shading in all images is on a logarithmic scale. *Top left*: Continuum-subtracted [O III] λ5007 image. The shading ranges between 8×10^{-18} (*white*) and 3×10^{-16} (*black*) ergs cm^{-2} s^{-1} pixel^{-1}. *Top right*: Continuum-subtracted Hα image. The shading ranges between 2×10^{-18} (*white*) and 3×10^{-16} (*black*) ergs cm^{-2} s^{-1} pixel^{-1}. *Lower left*: Image through F547M filter (continuum). The shading ranges between 6×10^{-17} (*white*) and 4×10^{-15} (*black*) ergs cm^{-2} s^{-1} pixel^{-1} in the filter band. *Lower right*: Image through F814W filter (continuum). The shading ranges between 1.5×10^{-16} (*white*) and 1.5×10^{-14} (*black*) ergs cm^{-2} s^{-1} pixel^{-1} in the filter band.

reveals a broad, spiral dust band that sweeps south from the intersection of the PC and upper right WF chips and then turns east and northeast, passing across the point at which the four chips intersect and continuing to the left-hand edge of the lower left WF chip. This dust lane coincides with a region of weak Hα emission between the two diffuse patches noted above and the central, bright region of the galaxy. The dust lane may obscure line emission in this region (where the four chips meet).

Figure 2 shows only the PC chip; the [O III] λ5007 image is top left, Hα is top right, *V* band is lower left, and *I* band is lower right. Figure 3 is an color display of the PC image of Hα. The [O III] λ5007 image contains a V-shaped structure (see also Fig. 5) within 2″ of the nucleus, plus fine-scale radial features extending to the northwest. There are also concentrations of bright, high excitation line emission toward the top of the panel, with an overall morphology suggestive of an elliptical ring, which might represent the projection of the end of a tilted, hollow, conical structure, with apex near the nucleus. In addition to the emission from H II regions ionized by hot stars (discussed below), the Hα image reveals prominent emission from the [O III]–emitting gas, including the V-shaped nuclear structure and the radial features and blobs to the northwest. The fainter [O III] λ5007 emission further to the northwest , imaged by Veilleux & Bland-Hawthorn (1997), is off the top edge of the PC chip.[4]

[4] It was, unfortunately, not possible to specify a special orientation of *HST* during these observations in view of our use of the Continuous Viewing Zone

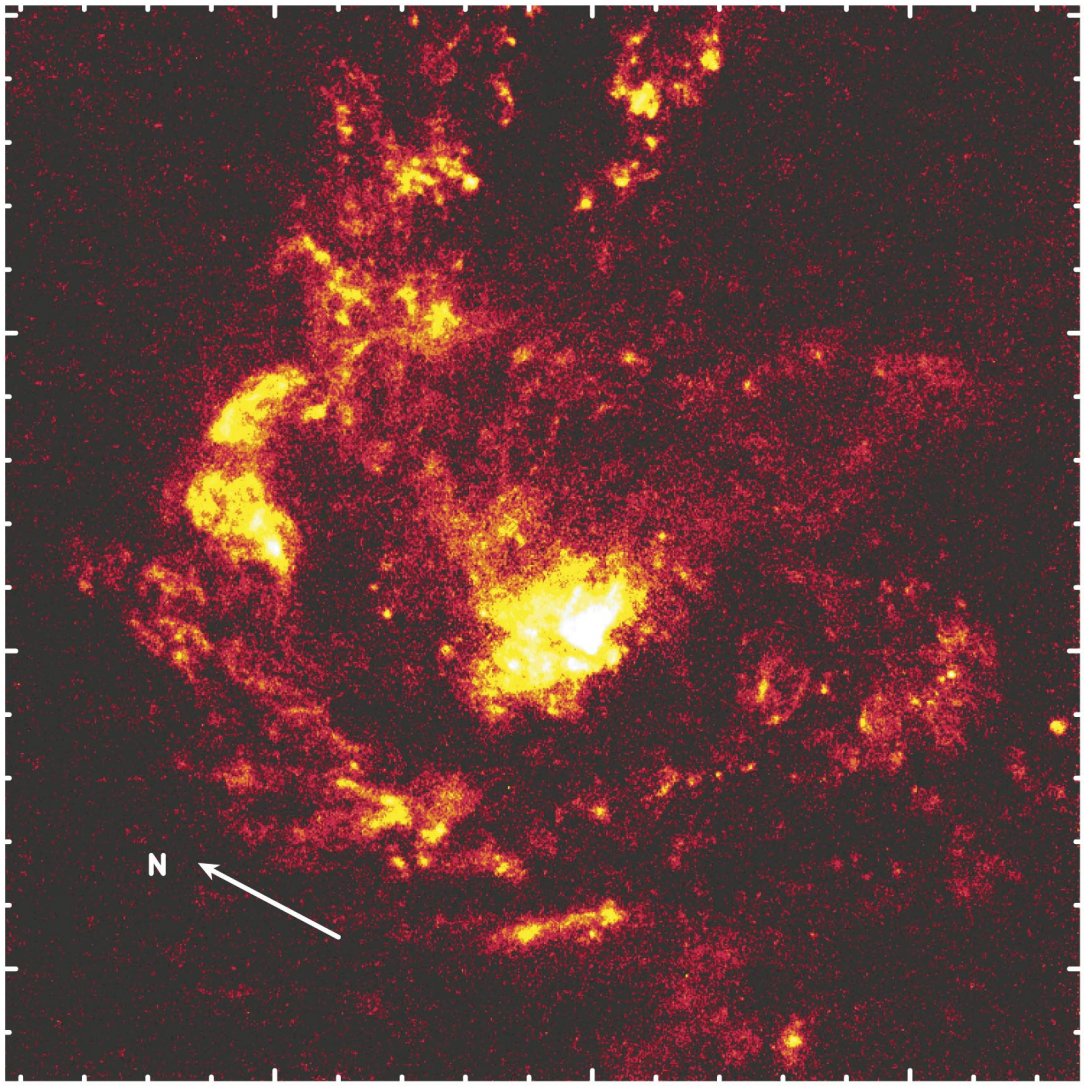

FIG. 3.—*HST* color image of the Hα emission of the Circinus galaxy, showing the PC only. Long tick marks are separated by 10″ and short tick marks by 2″. A long tick mark on each axis is aligned with the apex of the "ionization cone," which can be seen as the brightest region in the center of the image. The field and orientation are the same as in Fig. 2.

The Hα image (Fig. 2, *top right*; Fig. 3) reveals the well-known ring of H II regions of radius 8″–14″. The ring shows considerable structure, some of which results from obscuration. For example, a prominent dust band, best seen in the *V*-band image (Fig. 2, *bottom left*), extends northeast–southwest 2″–8″ south of the nucleus. The sharp northwest edge of this band is seen as a sharp edge in the Hα emission some 9″ southwest of the nucleus. Indeed, the Hα line emission is weaker and more fragmented to the south of the nucleus than in other directions, apparently a result of obscuration by the dust band. Various other dust bands, extending northeast–southwest to the southeast (*bottom of panel*) of the nucleus, are seen in the *V*- and *I*-band (*bottom right*) images. Given the projected shape of this ring of H II regions, it cannot be an intrinsically circular structure in the plane of the galaxy disk. Close to the nucleus, the Hα image also shows an elliptical ring of H II regions with radius 2″ toward the northeast (best seen in Figs. 5 and 12, below). We shall refer to this feature as the "nuclear ring." The nuclear ring extends more than half-way around the nucleus, from south through east to north of the nucleus, with major axis more or less along the galaxy disk (northeast–southwest). This morphology suggests the nuclear ring is intrinsically circular in shape and is located in the plane of the galaxy disk (§ 4.2).

The top panel of Figure 4 is an image of the flux ratio [O III] λ5007/Hα over the PC chip. We should bear in mind that this ratio can be measured only in the high-excitation gas, where both [O III] and Hα are detected. Elsewhere, in H II regions where [O III] is undetected, only an upper limit to the ratio is obtained (§ 2.1). This ratio is typically $\lesssim 0.5$ in the starburst ring, confirming the low excitation of the gas and commensurate with the values expected for H II regions. In the nuclear ring of H II regions, some 2″ northeast of the cone's apex, there is a light band where the upper limit to the ratio is lower at $\lesssim 0.1$–0.5. Extending more than 4″ northwest from the cone's apex are seen the high-excitation linear streamers and knots that stand out in the [O III] image (Fig. 2, *top left*). The ratio for the streamers within 10″ of the nucleus is lower than farther away; this might be a result of superposition on background H II regions, of reddening close to the nucleus, or of a lower ionization parameter due to a higher gas density near the nucleus. Beyond 10″, where the high-excitation gas projects

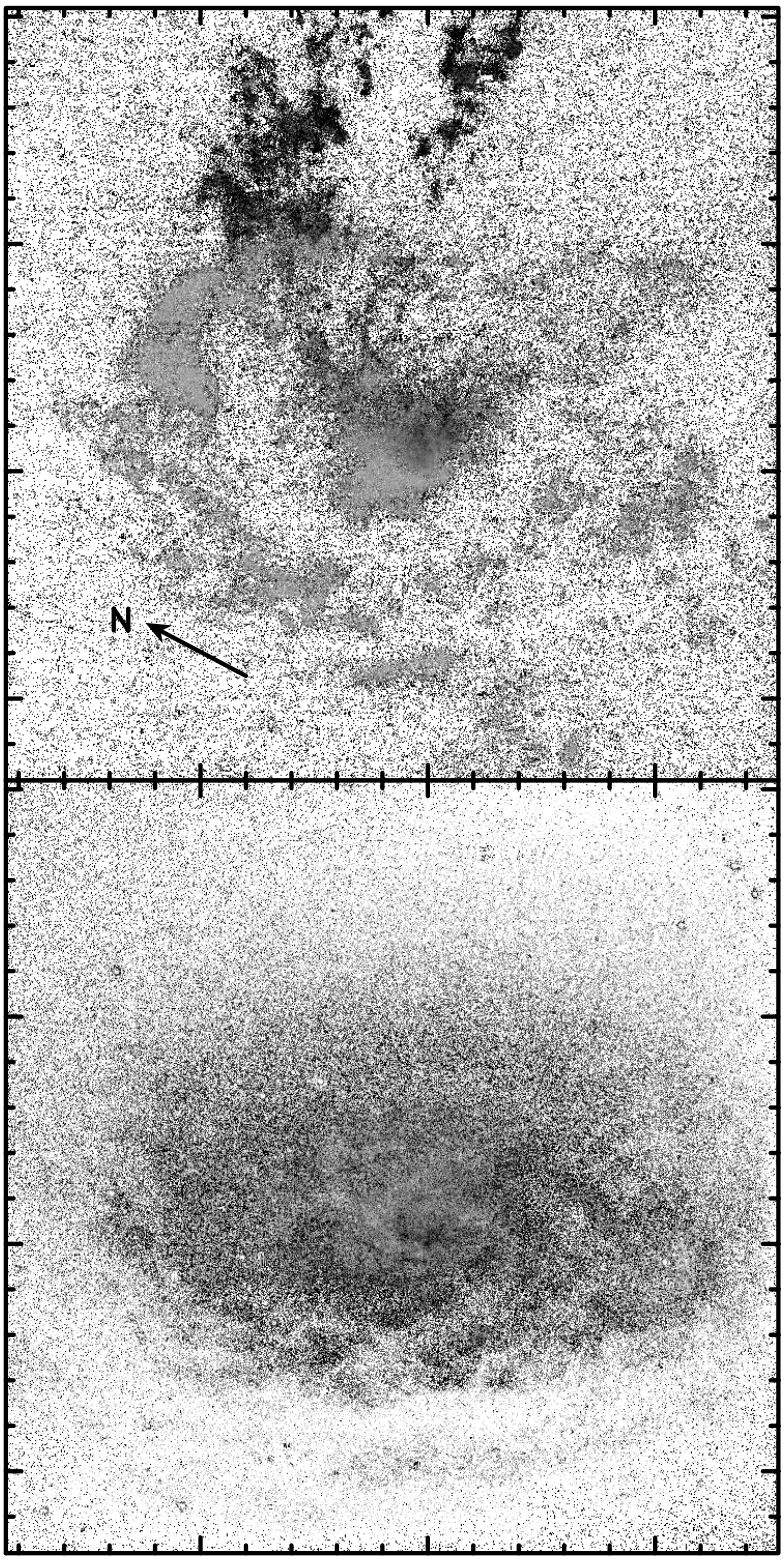

FIG. 4.—*HST* images of the Circinus galaxy, showing the PC chip only (see Fig. 2 for details of pixel size, scale, and orientation). *Top*: The [O III] λ5007 image divided by the Hα image. Darker shades represent higher ratios. The shades cover the range of ratios -1 (*white*) to 2 (*black*) on a linear scale. *Bottom*: $V-I$ color image. The shades range between $V-I=1.7$ (*white*) and 3.2 mag (*black*) and are linear in magnitude. Darker shades thus represent redder colors. Locations where the (noisier) V-band image has negative flux are colored white.

outside the starburst ring, the [O III]/Hα ratio of the streamers and knots ranges from 1 to ≥ 3, confirming that this gas has Seyfert-type excitation and suggesting that it is little reddened by dust internal to the Circinus galaxy. These [O III]/Hα ratios should be multiplied by 1.6 to correct for the foreground reddening of $A_V = 1.5$ mag (Freeman et al. 1977).

The lower panel of Figure 4 shows the ratio of the F547M and F814W images, which has been converted to a $V-I$ color map. This image shows considerable structure, espe-

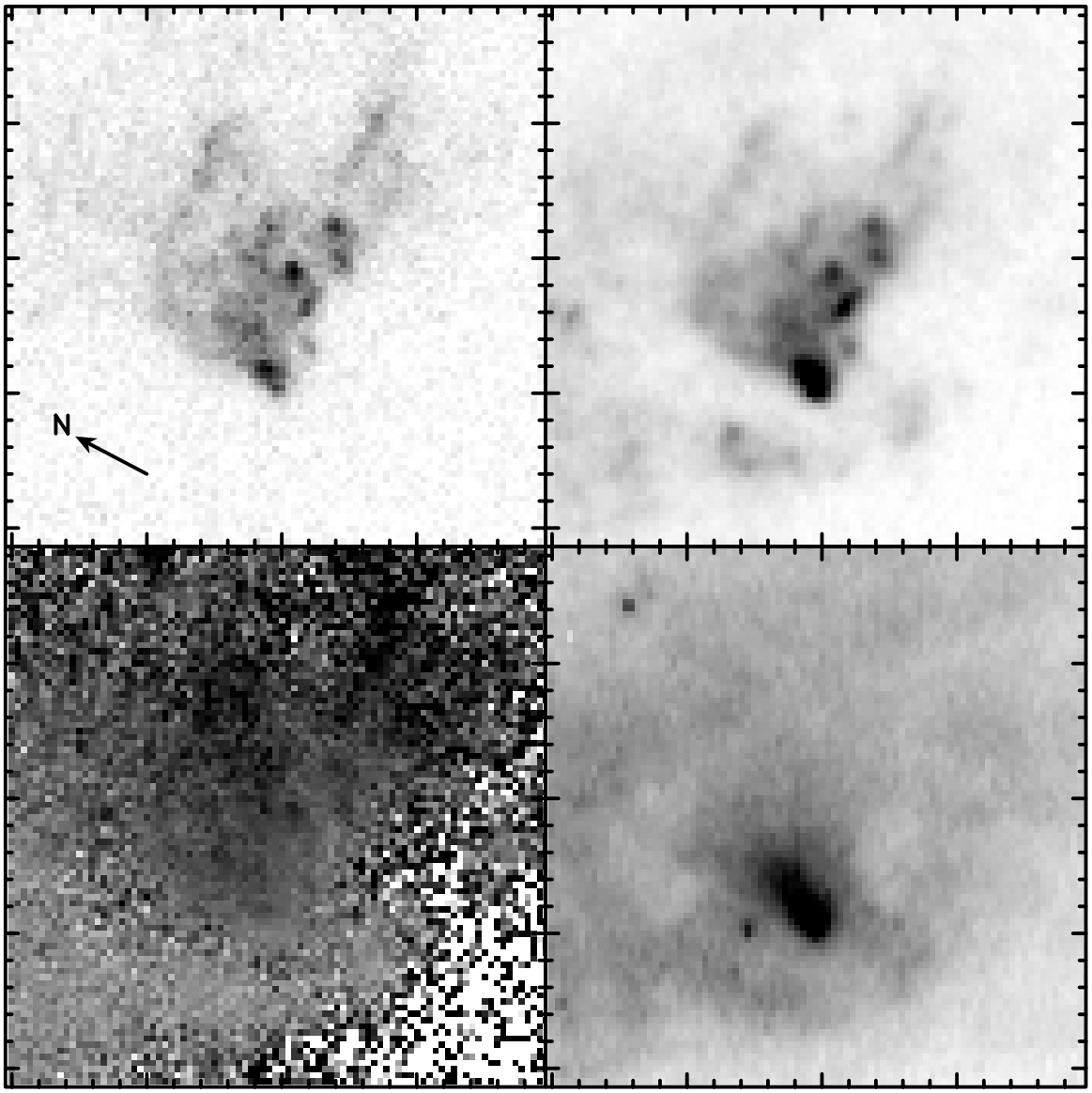

FIG. 5.—*HST* images with the PC of the nuclear region of the Circinus galaxy. Long tick marks are separated by 1″ and short tick marks by 0.″2. A long tick mark on each axis is aligned with the apex of the "ionization cone." The field of each panel is 4.″0 × 4.″0. The orientation and pixel size are the same as in Fig. 2. Darker shades represent higher values in all panels, and all shading is on a linear scale. *Top left*: Continuum-subtracted [O III] λ5007 image. The shading ranges between 1×10^{-18} (*white*) and 3×10^{-16} (*black*) ergs cm^{-2} s^{-1} pixel^{-1}. *Top right*: Continuum-subtracted Hα image. The shading ranges between 1×10^{-18} (*white*) and 3×10^{-16} (*black*) ergs cm^{-2} s^{-1} pixel^{-1}. *Bottom left*: The [O III] λ5007 image divided by the Hα image. The ratio is calculated for all areas with S/N ≥ 1 in both images. The ratio ranges from −1 (*white*) to 1.5 (*black*). *Bottom right*: Image through F814W filter (continuum). The shading ranges between 5×10^{-16} (*white*) and 7×10^{-15} (*black*) ergs cm^{-2} s^{-1} pixel^{-1} in the filter band.

cially on the near (southeast) side of the galaxy disk where red spiral bands are apparent. Regions as red as $V-I \simeq 3.2$ are found.

Enlarged views of the nuclear region (central 4.″0 × 4.″0) are shown in Figure 5. In both [O III] (*top left*) and Hα (*top right*), a filled V-shaped feature, with opening angle ≃90°, extends some 2″ to the northwest of the nucleus (taken as the apex of the V). The axis (i.e., the bisector of the edges) of the V is in PA ≃ −44°, which is 74° from the major axis of the galaxy disk and ≃64° from the optical continuum polarization direction at the nucleus (Oliva et al. 1998). The fact that the axis of the V is not perpendicular to the polarization is consistent with the conclusion that the polarization is dominated by transmission through aligned grains in the galaxy disk, rather than scattering within an ionization cone (Oliva et al. 1998). Considerable structure is found within the V, including knots, a straight streamer 2″ west of the nucleus and a curved streamer which extends first north from the nucleus and then turns west, ending 2″ from the nucleus (see also Fig. 12). The brightest emission within the V lies along its southern edge, adjacent to the detected H_2 $v = 1$–0 $S(1)$ emission (§ 3.2.3), perhaps indicating that the gas density is higher in this region than in other parts of the V. The bright, compact feature right at the apex of the V is elongated by ≃0.″3 in a north-northwest (PA −23°) direction. All structures within the V are clearly visible in both lines. The Hα image shows, in addition, emission outside of the V that is not seen in [O III] and presumably comes from H II regions. In particular, the nuclear ring of H II regions with radius 2″ (discussed above) is apparent, though better seen in Figure 12. The [O III]/Hα ratio map (Fig. 5, *bottom left*) confirms that the gas within the V has a higher excita-

tion than that outside of it. Both the straight streamer and the curved streamer noted above show up as high-excitation features. The low excitation of the gas in the nuclear ring, some $\sim 2''$ northeast of the nucleus, was noted earlier. The bright, elongated emission-line feature right at the apex of the V is also seen strongly in the *I*-band continuum (Fig. 5, *bottom right*), in which image it extends 0.″7 north-northwest of the nucleus, at the same PA ($-23°$) as found for Hα.

3.2. *Infrared Images*

3.2.1. *The Extended Infrared Continuum and Colors*

The *HST* continuum image obtained through the F215N filter is shown in Figure 6. Diffraction rings are clearly visible in all the *HST* infrared images, indicating a strong contribution from an unresolved source at the nucleus (discussed in § 3.2.2) and confirming the finding of Maiolino et al. (1998). Figure 6 also shows the bright circumnuclear emission plus a series of alternating bright and dark spiral arms to the southeast, which are qualitatively similar to those seen in the *I*-band image (Figs. 1 and 2)

Figure 7 shows a color image made from our F547M (*blue*), F814W (*green*), and F204M (*red*) images and reveals a dramatic color gradient across the galaxy. The strong dust bands to the southeast have already been noted, and the red colors on this side are also indicative of obscuration. A color gradient from the near to the far side of the disk has also been found in $H-K$ color by Maiolino et al. (1998).

Figure 8 is a gray-scale image of the observed $V-K$ colors, derived from the F547M and F204M images. The reddest region is at the nucleus, where $V-K \simeq 8.0$. The near (southeast) side of the galaxy disk is much redder (shown as darker shades) than the far (northwest) side, as already noted from Figure 7. The redder regions on the near side of the galaxy disk correspond to $6.0 < V-K < 7.5$, while the bluer extended regions on this side range down to $V-K \simeq 4.2$. On the far (northwest) side, the colors are mostly in the range $4.0 < V-K < 5.0$, although redder regions ($5.0 < V-K < 6.0$) are also present. The foreground extinction to Circinus is $A_V = 1.5$ mag (Freeman et al. 1977), which corresponds to $E(V-K) = 1.3$ mag (Cardelli, Clayton, & Mathis 1989). Thus the bluest regions have intrinsic colors $V-K \leq 2.7$ mag, the equality applying if these regions suffer no extinction internal to Circinus. Assuming an intrinsic stellar color of $V-K = 2.7$ mag and that the dust lanes on the near side lie fully in front of these

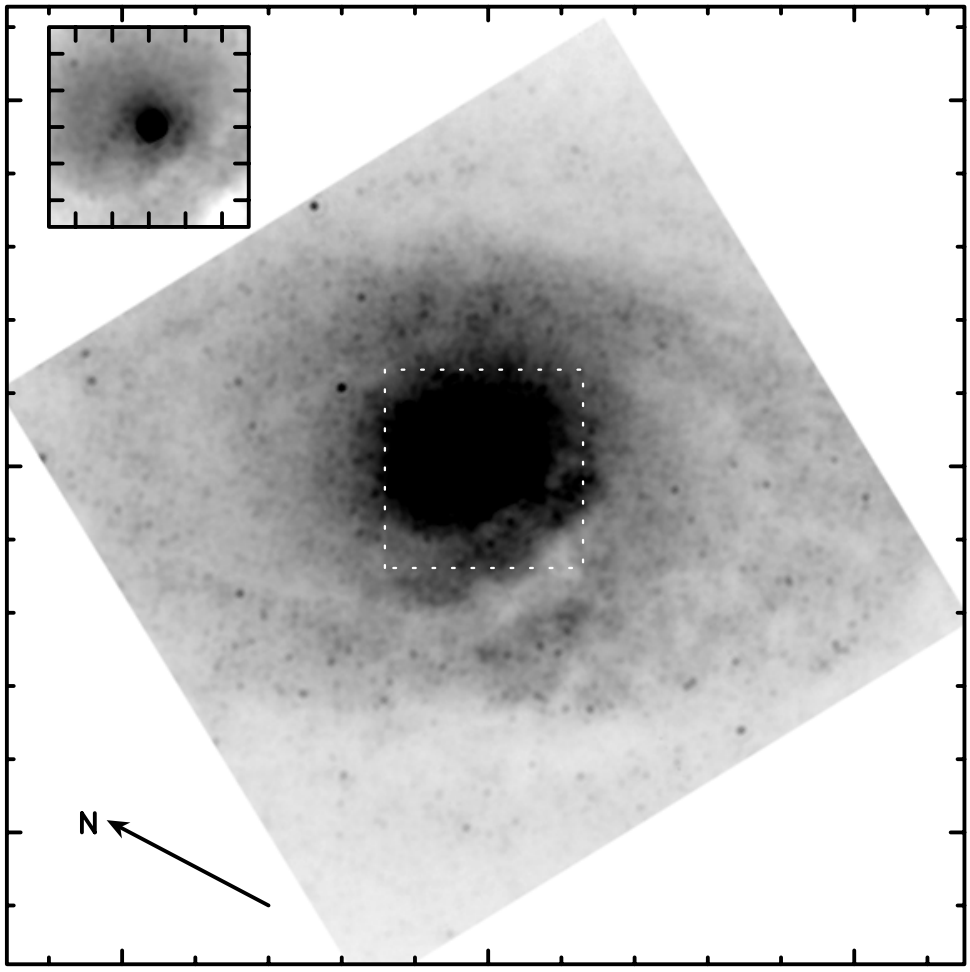

FIG. 6.—*HST* image of the near-infrared continuum of the Circinus galaxy obtained with NICMOS Camera 2 and filter F215N. The pixel size was rebinned to that of the PC (0.″0455), and the main image shows the full field (19.″2 × 19.″2) of the camera. Long tick marks are separated by 10″ and short tick marks by 2″. The orientation is the same as Fig. 2. Darker shades represent brighter regions. The shading in the main panel is on a linear scale and ranges between 0 (*white*) and 1.4×10^{-14} (*black*) ergs cm^{-2} s^{-1} μm^{-1} (PC pixel)$^{-1}$. The inset shows the area of the white dotted square with shading on a logarithmic scale between 0.6 (*white*) and 5.0 (*black*) $\times 10^{-14}$ergs cm^{-2} s^{-1} μm^{-1} (PC pixel)$^{-1}$. The peak flux is 68×10^{-14} ergs cm^{-2} s^{-1} μm^{-1} (PC pixel)$^{-1}$ The tick marks in the inset are separated by 1″.

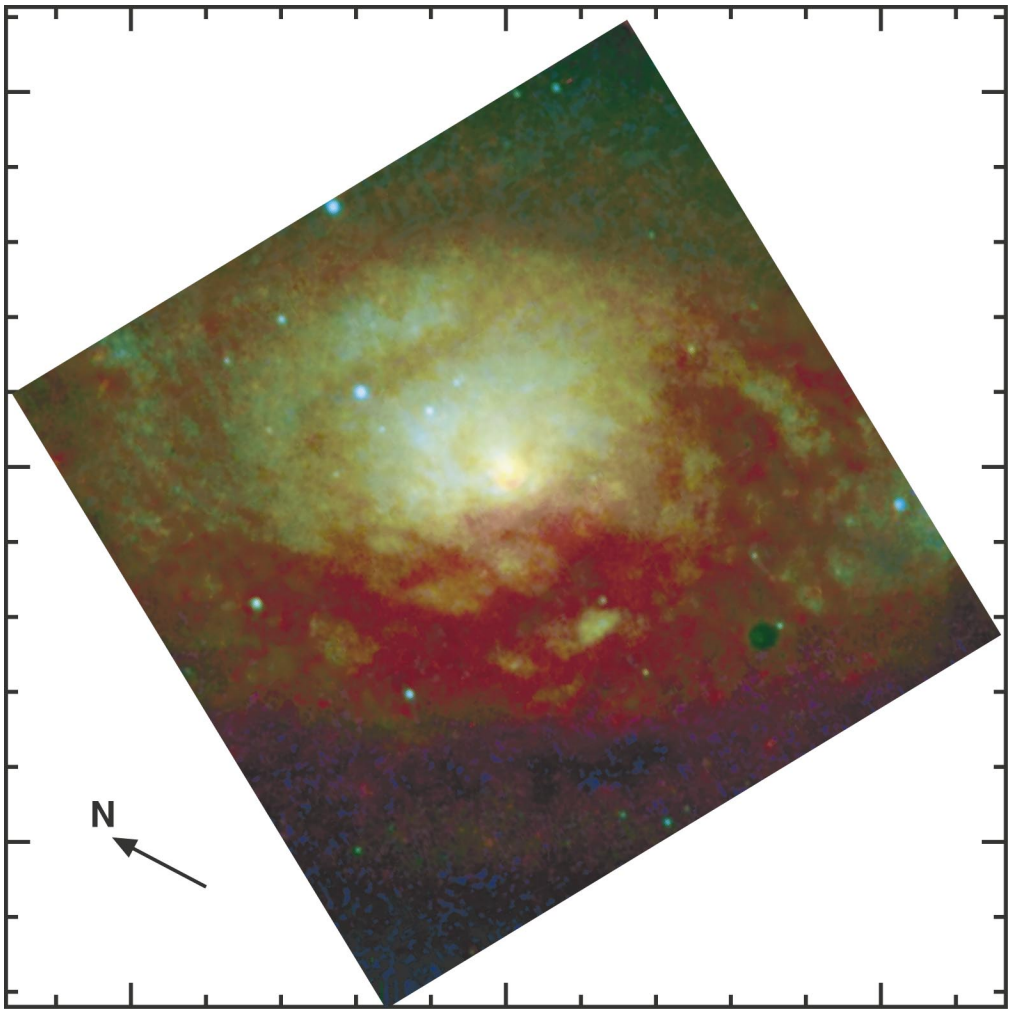

FIG. 7.—Optical–infrared color image of Circinus obtained from *HST* images through filters F547M (approximate *V*), F814W (approximate *I*), and F204M (within the *K* band). The image is 19″.2 on a side. Long tick marks are separated by 10″ and short tick marks by 2″. The orientation is the same as Fig. 2. The dark circle in the lower right is the coronographic hole. The color scheme is such that F547M is mapped to blue, F814W to green, and F204M to red. No correction has been applied for foreground reddening.

stars, the obscuration through the dust lanes is typically $2.2 < A_V < 3.9$ mag.

An intrinsic $V-K = 2.7$ mag is bluer than found in bulge-dominated galaxies: the average color for elliptical and lenticular galaxies is $V-K \simeq 3.3$ (Frogel et al. 1978). The H II regions and $J-K$ colors (Storchi-Bergmann et al. 1999) also indicate the presence of a young stellar population. The color $V-K = 2.7$ mag is, however, redder than all the starburst models of Leitherer & Heckman (1995), except high-metallicity, instantaneous bursts with age $\simeq 10^{6.9\pm0.1}$ yr. It is possible that the foreground extinction of $A_V = 1.5$ mag underestimates the extinction to the bluest regions and that their intrinsic $V-K < 2.7$. Alternatively, the observed starlight could represent a mixture of young disk and old bulge stars.

Any interpretation of the colors must also account for the strong tendency for dust lanes to be seen on the near side of the disk of Circinus and much less so on the far side. If all the starlight is from the disk, strong dust bands must lie between Earth and the stars in the galaxy disk on the near side, but not those on the far side. Outside corotation, the compression takes place on the outer edge of a spiral arm (since $\Omega_{\rm pattern} > \Omega_{\rm gas}$). On the near (southeast) side of the galaxy disk, the dust lanes associated with a spiral arm would then be nearer to Earth than the hot stars formed in the arm, an effect with the correct sense to account for the excess reddening on the near side. On the other hand, the highlighted dust lanes on the near sides of galaxy disks are usually understood as an effect of the dusty disk on background bulge light (Hubble 1943). This interpretation would require a significant contribution from bulge light in the inner few hundred pc of Circinus. It is not clear to us which of these two explanations for the excess of dust lanes and reddening on the near side of Circinus is the correct one.

3.2.2. *The Unresolved Nuclear Source*

We have used TINYTIM V4.4 to model the point spread function (PSF) of NICMOS camera 2. The flux density of the compact nuclear source was then obtained by two methods. In the first, we used the IRAF task sclean to perform a σ-CLEAN deconvolution (Keel 1991). The TINYTIM PSF was computed onto an oversampled grid of 11×11 elements per NIC2 pixel and then resampled to the actual pixel scale so as to allow us to simulate the source peak being located at different locations within the central pixel. The σ-CLEAN algorithm was run for all 121 such resampled PSFs, and the PSF that gave the largest

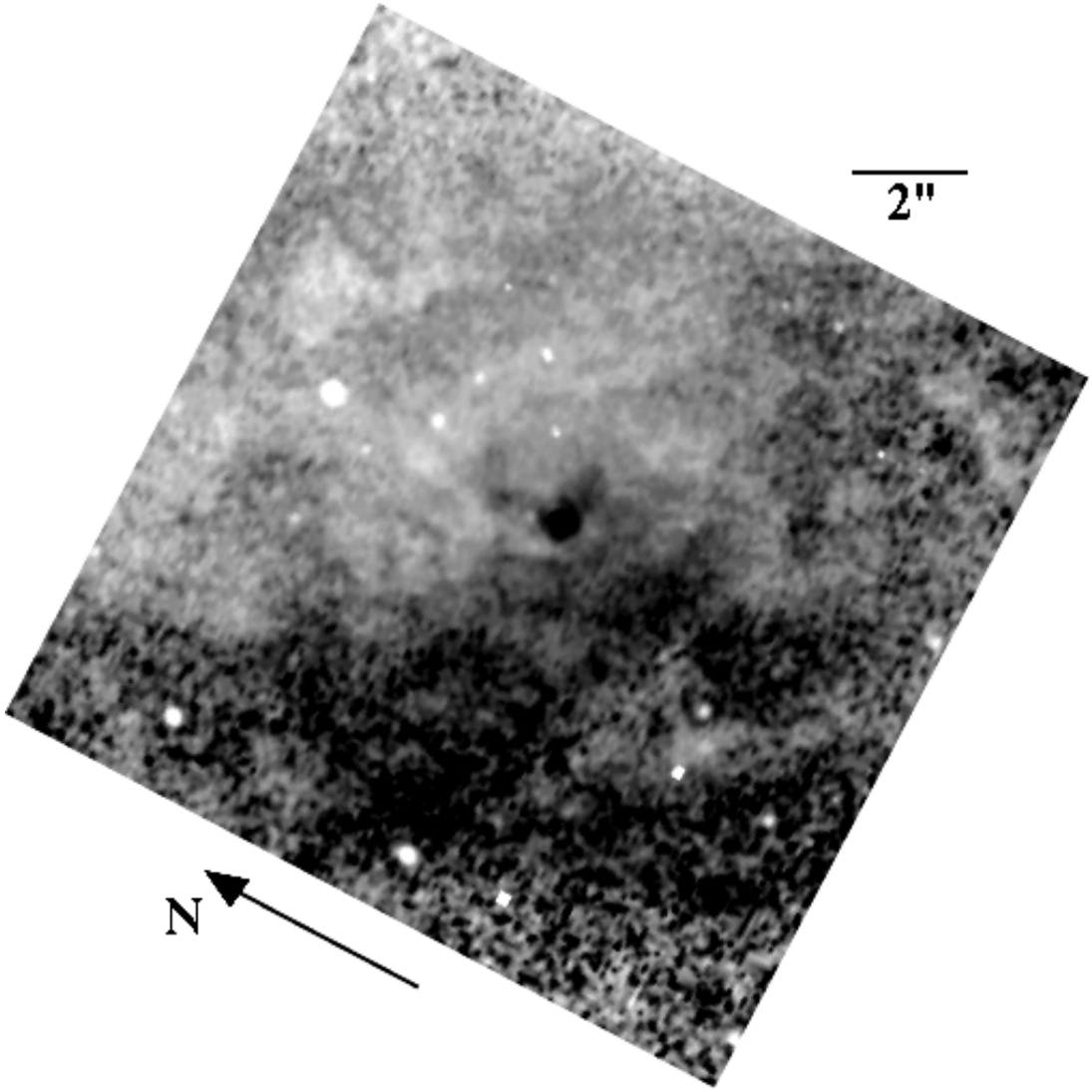

FIG. 8.—Gray-scale image of the $V-K$ colors of Circinus obtained from the F547M and F204M images. No correction has been applied for foreground reddening. Darker regions are redder; the reddest region is at the nucleus and has V–$K \simeq 8.0$, while the bluest region is to the northwest and has $V-K \simeq 4.0$. The orientation is the same as Fig. 2.

maximum pixel value in the final image was assumed to be the most accurate representation of the true PSF.

The second method involved fitting a de Vaucouleurs $r^{1/4}$ law to the azimuthally averaged radial surface brightness profile over the range of radii $0\farcs6 < r < 5''$, and then extrapolating this to smaller radii. We then scaled the PSF so that the sum of the two components matched the peak of the surface brightness. These results are shown in Figure 9.

The agreement between the flux densities of the compact nuclear source derived by the two methods is very good. The discrepancy exceeds 4% only in the F212N filter, where the presence of H_2 emission concentrated near the nucleus has presumably caused the profile fitting method to overestimate the true contribution of the point continuum source. We opt, therefore, to use the fluxes derived from the σ-CLEAN deconvolution to investigate the nature of the nucleus and assume internal errors of 5% on both the F204M and F215N measurements.

However, comparison of our flux-calibrated NICMOS images with ground-based measurements (Moorwood & Glass 1984; Glass & Moorwood 1985) indicates a systematic discrepancy between the two sets of photometry. Our F212N and F215N images are brighter by 31% and 32%, respectively, in all apertures, while the nucleus contributes only 4%–10% of the total light, depending on the aperture size. Our F204M image is brighter by 23% assuming a flat spectrum in the K band, although the true discrepancy will be slightly larger as the flux density of Circinus increases with wavelength (Storchi-Bergmann et al. 1999). There thus appears to be a systematic offset of $\sim$30% in the NIC2 photometry for these three filters. We have, therefore, reduced all flux measurements by 30%, and the resulting flux densities of the point source are listed in Table 1. Our estimate of the point source flux is in line with that of Maiolino et al. (1998), who found 24 mJy at K ($\lambda_{\rm eff} = 2.2$ μm).

The observed F215N$-$F204M color can be reproduced by a power law with a spectral index $\alpha_o = 7.0 \pm 1.2$ ($S_\nu \propto \nu^{-\alpha}$); the L' (3.8 μm) flux measured by Maiolino et al. (1998) agrees with the extrapolation of this spectrum. If we assume that this steep spectrum is the result of a heavily reddened, much shallower power law, it is possible to infer the obscur-

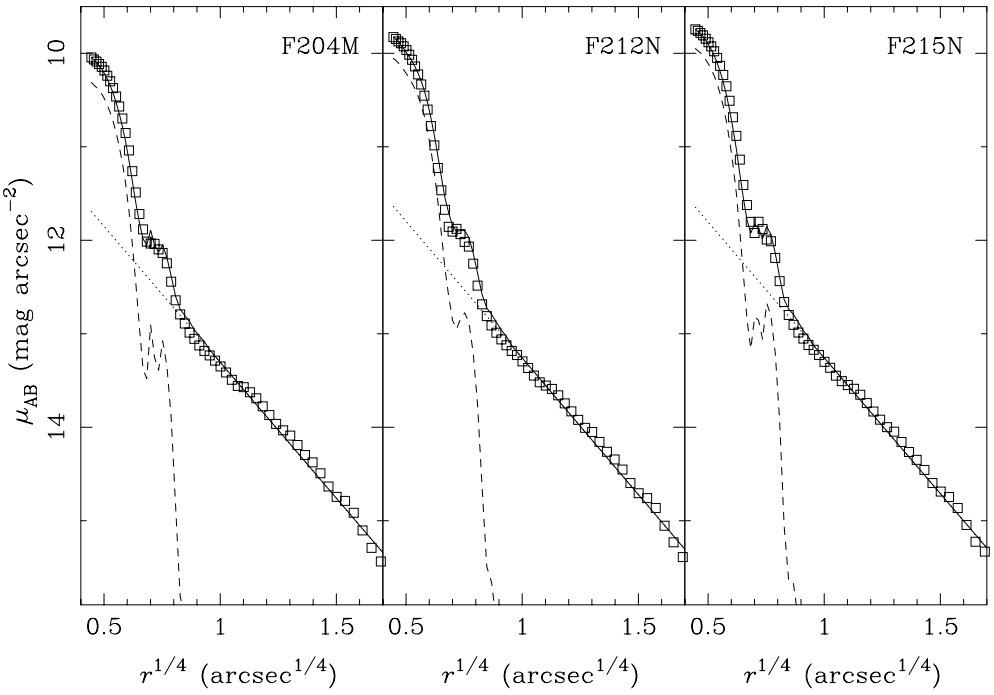

FIG. 9.—Radial surface brightness profiles of Circinus in the three NICMOS filters. The dotted lines represent the results of fitting a de Vaucouleurs $r^{1/4}$ law to the region $0\farcs6 < r < 5''$, and the dashed line is the point-spread function scaled so that the sum of the two components (the solid line) matches the peak of the observed emission. The flux density scale has not been corrected for the suspected systematic error in the NICMOS fluxes (see text) and thus may be 30% too high.

ation, A_V, as a function of the intrinsic spectral index, α_i, as shown in Figure 10. Fadda et al. (1998) find that the spectral index of Seyfert 1 galaxies at K band is $\alpha_i \simeq 1.8$. If the unresolved infrared source in the nucleus of Circinus is actually an obscured Seyfert 1 nucleus with this value of α_i, then the foreground extinction is $A_V = 28 \pm 7$ mag. This value is in excellent agreement with the optical depth of the 9.7 μm silicate feature observed by Moorwood & Glass (1984), assuming an underlying blackbody spectrum and $A_V/\tau_{9.7} = 16.6$ (Rieke & Lebofsky 1985) and is also consistent with the $A_V \sim 20$ mag inferred by Marconi et al. (1994). Applying a correction of $A_V = 28$ mag, the unobscured 2.2 μm flux of the nucleus would be 446 mJy.

The extinction to the near-infrared nucleus is much lower than expected from the gas column of 4×10^{24} cm^{-2} to the nuclear X-ray source (Matt et al. 1999). Assuming a normal gas-to-dust ratio, the implied extinction is $A_V \sim 2000$ mag or $A_K \sim 230$ mag. This difference indicates that the near-IR continuum originates in regions farther from the nucleus than the X-rays, most probably being reemission of nuclear radiation by dust. As the near-IR source is unresolved, the radius of the reemitting structure is smaller than 2 pc and could be the inner regions of a torus. Alternatively, the inner regions of the torus may have an obscuration similar to that of the X-ray source and thus be invisible in the near-infrared. The observed K-band light could then originate from hot dust in the inner part of the narrow-line region, perhaps along the polar axis of the torus and heated by

TABLE 1

FLUX DENSITIES OF THE NUCLEAR COMPONENT IN THE THREE NICMOS FILTERS

		NUCLEAR FLUX (mJy)	
FILTER	λ_{eff} (μm)	SCLEAN	Profile
F204M.....	2.0355	15	15
F212N	2.1213	21	23
F215N	2.1487	21	22

NOTE.—Flux densities were derived using SCLEAN and by fitting a point source plus stellar bulge to the observed radial surface brightness profile. A correction for the apparent systematic error in the flux calibration of NIC2 has been applied (see text).

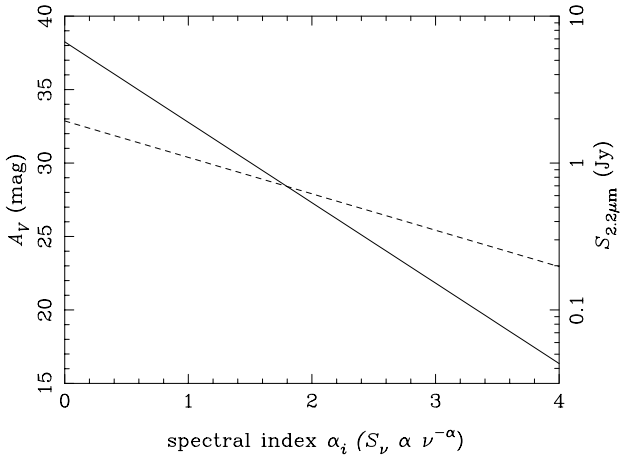

FIG. 10.—Plot of visual obscuration, A_V (*left axis* and *solid line*), against intrinsic spectral index, α_i, for the nucleus of Circinus. The right axis and dashed line show the corresponding intrinsic flux density at 2.2 μm. This flux density scale has not been corrected for the suspected systematic error in the NICMOS fluxes (see text) and thus may be 30% too high. The extinction law of Cardelli et al. (1989) has been used.

nuclear optical–UV light or mass outflow, as may be the case in NGC 1068 (Braatz et al. 1993; Weinberger, Neugebauer, & Matthews 1999). Such a geometry provides a natural explanation for the lower obscuration to the near-infrared source than to the hard X-ray source. Other explanations for a large N_H/A_V ratio found in a Seyfert 2 galaxy are discussed in Simpson (1998).

The absorption-corrected K-band and 2–10 keV luminosities of the compact nucleus are $L(K) \simeq 2.4 \times 10^{41}$ ergs s^{-1} and $L(2\text{–}10\ \text{keV}) = 3.4 \times 10^{41}$ to 1.7×10^{42} ergs s^{-1} (Matt et al. 1999), respectively. These numbers agree well with an extrapolation to lower luminosities of the correlation between $L(K)$ and $L(2\text{–}10\ \text{keV})$ for hard X-ray–selected active galaxies, mainly Seyfert 1 galaxies (Kotilainen et al. 1992, their Fig. 7*c*). This agreement supports the view that Circinus contains a Seyfert 1 nucleus with different obscuring columns to the K-band and hard X-ray sources. It also indicates that the hot dust radiating in the near-infrared "sees" the dust-heating source (i.e., the compact optical, UV, and X-ray source) through a smaller column of gas than we do.

3.2.3. *The Molecular Hydrogen Emission*

The continuum-subtracted image of the H_2 $v = 1\text{–}0$ $S(1)$ emission line is shown in Figure 11. Unfortunately, the strong contribution from the point source results in significant residual artifacts at and near the nucleus. Attempts to remove these, by subtracting a scaled PSF from the images before combining them, did not prove successful, and we are therefore unable to learn anything about the structure of the H_2 emission closer than 0.″5 from the nucleus.

The molecular hydrogen extends toward the west-southwest of the nucleus, in agreement with the inner part of the image in the same line presented by Maiolino et al. (1998). We fail to detect the much fainter, more extended emission seen by Maiolino et al. (1998), Davies et al. (1998), and Storchi-Bergmann et al. (1999). The H_2 is strongest outside, and to the south, of the V-shaped region of high-excitation ionized gas (compare Figs. 5 and 11, which have the same field size and orientation), confirming the recent findings of Maiolino et al. (2000) from a ground-based image in the same line.

The molecular hydrogen emission $\simeq$0.″75 to the west-southwest of the nucleus is at least 3 times brighter than that at the same distance east-northeast of the nucleus. If the distribution is intrinsically symmetric, but the eastern emission is obscured, a minimum of 1.2 mag of extinction at 2.12 μm would be required, corresponding to $A_V \gtrsim 10$ mag. This is consistent with the extinction we derived to the nuclear infrared continuum source (§ 3.2.2), and so we may

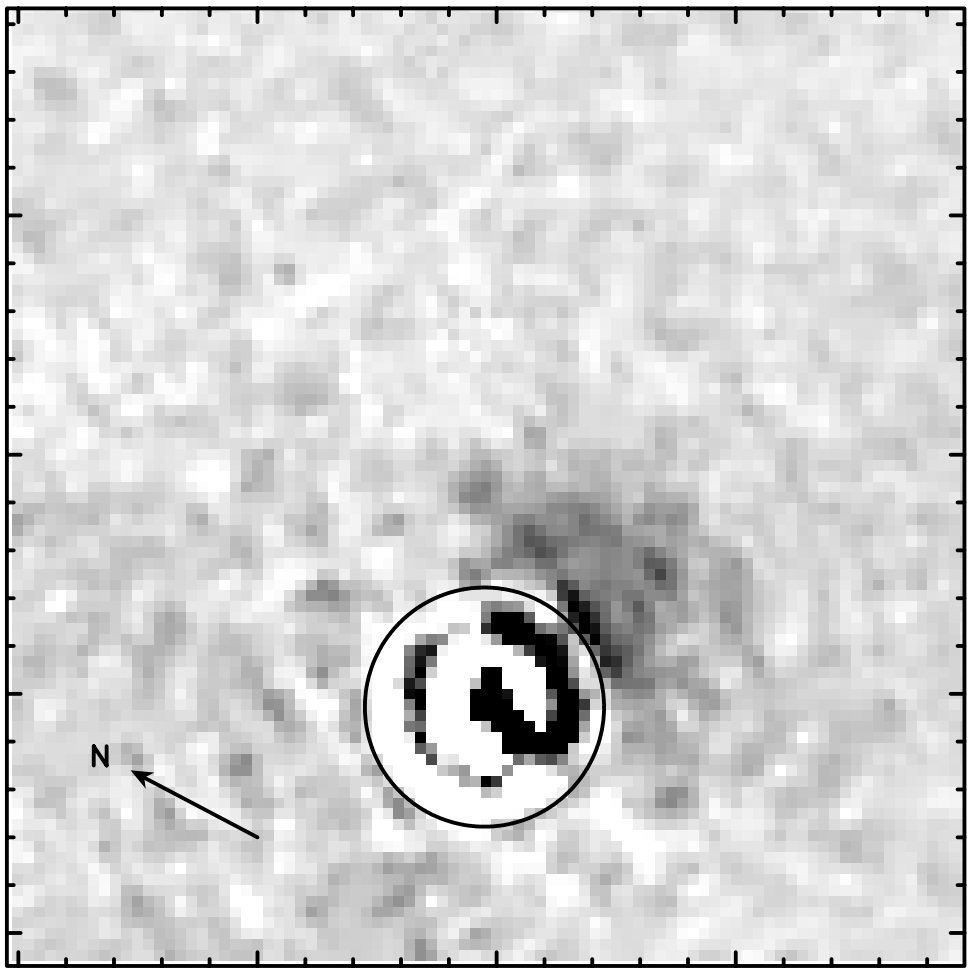

FIG. 11.—Image of the H_2 $v = 1\text{–}0$ $S(1)$ line, obtained by subtracting the continuum from the F212N image (see text). Long tick marks are separated by 1″ and short tick marks by 0.″2. The field of view and orientation are the same as in Fig. 5. Darker shades represent brighter regions. Structure inside the circle, which is centered on the bright, nuclear continuum source, is unreliable (see text).

be observing the effects of a large-scale obscuring structure close to the plane of the galactic disk (McLeod & Rieke 1995; Simcoe et al. 1997). Alternatively, of course, there may simply be more molecular gas, or its temperature and/or density may be more conducive to emission in the H_2 $v = 1$–0 $S(1)$ line, to the west of the nucleus than to the east.

3.2.4. *The* [Fe II] *Emission*

A contour map of the [Fe II] $\lambda 1.644$ μm line is shown superposed on the *HST* Hα image in Figure 12. There is a compact source (flux 3.2×10^{-14} ergs cm^{-2} s^{-1}), which we presume coincides with the nucleus, plus an extended arclike feature (flux 1.8×10^{-14} ergs cm^{-2} s^{-1}) to the northeast. Faint [Fe II] emission is also associated with a spiral arm some 5″– 7″ to the east and southeast of the nucleus. Our image and fluxes are broadly consistent with those obtained by Davies et al. (1998) in the same line, though their resolution was lower and the arclike feature is seen in their image as a small extension of the nucleus to the northeast. This arclike feature coincides with, and is morphologically similar to, the northeast part of the nuclear ring of H II regions seen in Hα (§ 3.1). The [Fe II] emission in the arc then presumably originates from shock excitation in supernova remnants. A weak radio continuum source coincides with the [Fe II] arc (Davies et al. 1998). The [Fe II] luminosities of the arc and the nucleus lie somewhat below the extrapolation to lower luminosity of the best fit to the empirical correlation between [Fe II] and radio luminosity found by Forbes & Ward (1993) and Simpson et al. (1996) for Seyfert and starburst galaxies. However, the Circinus values are consistent with the correlation given its scatter. The observed 3″ (60 pc) length of the arc rules out the suggestion (Davies et al. 1998) that all the [Fe II] emission comes from a single, young supernova remnant. However, Maiolino et al. (2000) find that the brightest [Fe II] emission of the arc is compact in *HST* images, with a size less than 4 pc, and argue that it may trace a single supernova remnant.

The origin of the [Fe II] associated with the nucleus itself is less clear, but Storchi-Bergmann et al. (1999) have found that the [Fe II] $\lambda 1.257$/Paβ ratio is $\simeq 0.4$ at the nucleus and increases outward. This low nuclear [Fe II] $\lambda 1.257$/Paβ ratio is typical of starbursts (Colina 1993; Simpson et al. 1996), so it may be that all the [Fe II] emission in the inner regions of Circinus—nucleus, arc, and spiral arm—is dominated by supernova remnants. This result may be contrasted with the situation in the nucleus of NGC 1068, where

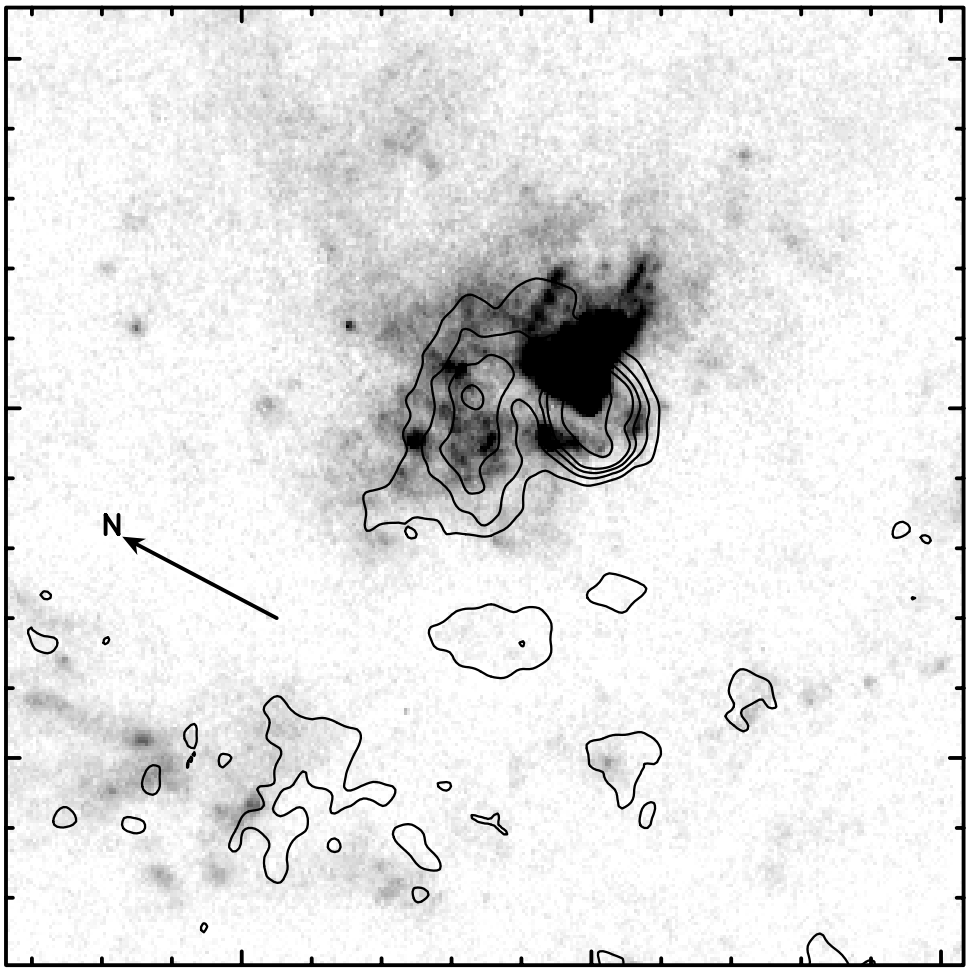

FIG. 12.—Contours of [Fe II] $\lambda 1.644$ μm emission superposed on a gray scale of the *HST* Hα image. Long tick marks are separated by 5″ and short tick marks by 1″. The field of view is 13.″7 × 13.″7, and the orientation is the same as Fig. 2. Darker shades represent brighter regions, and the shading is on a linear scale from 2×10^{-18} (*white*) to 8×10^{-17} (*black*) ergs cm^{-2} s^{-1} PC pixel^{-1}. The contours of [Fe II] emission are plotted at (5, 10, 15, 20, 40, 60, 80, and 100) $\times$ 1.69×10^{-16} ergs cm^{-2} s^{-1} (arcsec)$^{-2}$. The images were superposed by aligning their peaks; this alignment is arbitrary. The arc of [Fe II] emission 2″ northeast of the nucleus is associated with an elliptical ring of H II regions with observed major axis along the galaxy disk.

Blietz et al. (1994) have found that the [Fe II] emission is elongated along the radio jet and may be powered by jet-driven shocks or photoionized by the active nucleus.

4. DISCUSSION: GAS IN THE INNER 100 pc OF THE CIRCINUS GALAXY

4.1. *The V-shaped High-Excitation Gas*

We have discovered a compact ($\simeq$30 pc), sharply bounded, filled V-shaped region of high-excitation gas (Figs. 5 and 12). This gas extends to the northwest and projects in the same direction as the larger scale ($\sim$500 pc) "ionization cone" (Marconi et al. 1994; Veilleux & Bland-Hawthorn 1997; Elmouttie et al. 1998b). Both the large-scale and small-scale "cones" undoubtedly extend out of the galaxy disk and are visible because they project against the far side of the disk; any countercone is obscured by dust in the disk. The opening angle of the compact V is $\simeq 90^\circ$, and the projections of its edges to larger radii fully envelop the more extended high-excitation gas. It is thus entirely possible that the compact V represents the projection of a "classical ionization cone"—ionizing photons escaping anisotropically from an unresolved source of ionizing photons. This collimation can result from either shadowing of an isotropic ionizing source by an optically thick torus of gas and dust or intrinsic anisotropy of the continuum source (e.g., Wilson 1992). The V-shaped structure extends down to our resolution ($\leq 0\farcs1$; see Figs. 5 and 12), so the collimation must occur on scales less than 2 pc. Krolik & Begelman (1988) state that the position of the inner edge of the torus is determined by a balance between the inward flow of clouds and the rate at which the nuclear continuum can evaporate them. They estimate that the radius of the inner edge is a few times S, where

$$S = 0.26 L_{44} \left(\frac{L}{L_E}\right)^{-3} \left(\frac{T_C}{3 \times 10^7 \text{ K}}\right)^{-2} \text{ pc}. \quad (1)$$

Here L_{44} is the central luminosity in units of 10^{44} ergs s^{-1}, L_E is the Eddington luminosity, and T_C is the Compton temperature. According to Moorwood et al. (1996), the total luminosity of the Seyfert nucleus is $\simeq 4 \times 10^{43}$ ergs s^{-1}. If $T_C = 3 \times 10^7$ K, then L/L_E must be $\gtrsim 0.7$ given our upper limit of 1 pc for the inner radius, which we have taken to be $3 \times S$. This means that the mass of the central black hole would have to be $M_{BH} \leq 5 \times 10^5\ M_\odot$ for Krolik & Begelman's description to be valid, a rather stringent limit. If $T_C \leq 3 \times 10^7$ K, the upper limit becomes lower. The limit on M_{BH} is stricter than the dynamically measured upper limit to the black hole mass of $M_{BH} \leq 4 \times 10^6\ M_\odot$ (Maiolino et al. 1998).

There are clear indications that the simplest picture—an anisotropic ionizing source illuminating ambient gas—is inadequate. First, kinematic measurements (Veilleux & Bland-Hawthorn 1997; Elmouttie et al. 1998b) show that the gas in the large-scale cone is outflowing. Radio maps show polar radio lobes fueled by outflow from the nuclear region (Elmouttie et al. 1998a). Second, our [O III] image suggests that the high-excitation gas some 200–400 pc from the nucleus takes the form of a roughly elliptical annulus (Fig. 2, *upper left*), suggesting we are viewing the open end of an inclined, circular conical structure extending roughly perpendicular to the galaxy disk. The cone at this radius seems to be hollow in the [O III] image, presumably as a result of a low-density outflowing wind or radio jet that has entrained dense gas along its edges, perhaps from the same compact dense torus that is supposed to collimate the ionizing radiation. Third, the existence of this outflow is a potential source of ionizing photons through photoionizing shocks (e.g., Dopita & Sutherland 1995). The outflow velocities observed—150–200 km s^{-1}—are, however, rather low for production of a significant ionizing luminosity, but higher velocity, lower density gas may also be present.

It is in principle possible that V-shaped structures, such as that seen in Circinus, simply represent gas seen along low-obscuration lines of sight, with high obscuration to either side. We do not favor this idea because of the alignment of the compact V with the larger scale, high-excitation gas, which is essentially unobscured. The region between the obscuring structures (i.e., the compact V) would have to be aligned by chance with the larger scale gas in such a picture. We thus conclude that the compact V is either a classical (ionization-bounded) ionization cone or a matter-bounded outflow with impressively straight edges.

4.2. *The Compact Circumnuclear Star-forming Ring*

Our Hα image shows the well known ring of H II regions with radius 150–270 pc (Figs. 2 and 3). This image also reveals a much more compact (radius 40 pc toward the northeast), clumpy structure of H II regions, which appear to form more than half of a nuclear ring (§ 3.1; Figs. 5 and 12). All of the compact V of high-excitation gas projects inside the ring. However, the ring is not exactly centered on the apex of the V. The major axis of the nuclear ring lies in PA $\sim 30^\circ$, close to the major axis of the disk. Further, the major-to-minor axial ratio of the approximately elliptical ring is $\sim$2.3, which corresponds to an inclination of $i_r \sim 64^\circ$ if the ring is intrinsically circular. This inclination is identical to the inclination of the large- scale stellar disk—$i_d = 65^\circ \pm 2^\circ$ (Freeman et al. 1977). This agreement between both the major axis and inclination for the compact ring and large-scale stellar disk indicates that we are dealing with an intrinsically circular ring in the plane of the disk. The two star-forming rings probably represent dynamical resonances (e.g., Buta 1995) and may result from gas being forced from farther out in the galaxy toward the nucleus by oval distortions or bars, such as the 100 pc long gaseous bar claimed by Maiolino et al. (2000).

It is also of interest to ask how close to the nucleus we see H II regions. The southern part of the ring projects to within 5 pc of the apex of the ionization cone (Fig. 12). However, if our interpretation is correct, the inner edge of the nuclear ring is actually at least 15 pc from the apex. There is fainter Hα emission between the ring and the cone's apex, but it is rather smoothly distributed and could be gas ionized by the hot stars which are presumably present in the ring. We find no conclusive evidence for hot stars within $\sim$10 pc of the nucleus, so models of starbursts within this region (Maiolino et al. 1998) should be treated with caution.

5. CONCLUSIONS

Our optical and infrared *HST* images of the Circinus galaxy reveal a wealth of detail. There is a sharp morphological distinction between the high-excitation ionized gas associated with the Seyfert activity and the low-excitation gas in H II regions ionized by hot stars. The infrared image in H_2 $v = 1$–0 $S(1)$ reveals the morphology of the warm molecular gas 10–20 pc from the nucleus. Our continuum images at V, I, and K bands provide information on the

stellar distribution, obscuring dust features and the compact nuclear continuum source. We discuss each of these components in turn.

1. *The high-excitation gas.*—On the smallest resolvable scales, there is a very bright feature extended by 0.″3 (6 pc; see Fig. 5). It is at the apex of a compact (2″ $\simeq$ 40 pc), filled, V-shaped region of emission, which is presumably conical or wedge-shaped in three dimensions. The coincidence of the bright feature with the cone's apex suggests that it marks the position of the nucleus. The filled V-shaped structure has an opening angle of $\simeq 90°$ and is brightest on its south side, adjacent to the brightest H_2 $v = 1$–0 $S(1)$ emission. The filled V may be a "classical" ionization cone (i.e., an ionization-bounded structure illuminated by an anisotropic nuclear source) or a matter-bounded region with impressively straight edges. The length of the V (~ 40 pc) is consistent with expectations for the half-thickness of the galaxy's gas disk, so we are observing the interaction of the Seyfert nucleus with the normal gas disk, before the ionizing radiation and outflow break out into the galactic halo. Extension of the arms of the V to larger radii encompasses the high-excitation gas previously imaged in ground-based observations. This alignment is consistent with the ionization-bounded interpretation in which anisotropic nuclear radiation photoionizes the high-excitation gas on all scales. The structure that collimates the ionizing photons is unresolved by our observations and must thus be less than 2 pc in extent. At 10″–20″ (190–380 pc) from the nucleus, the morphology of the high-excitation gas is suggestive of an elliptical ring (Fig. 2), which we interpret as emission from the edges of a circular conical structure viewed at an oblique angle. This concentration of gas on the edge of the cone suggests entrainment of dense gas, presumably in the disk of the galaxy, which is then carried out of the galactic disk by a lower density wind, which may also power the radio lobes.

2. *The* H II *regions.*—On the smallest scales, we find a partial elliptical ring (Figs. 5 and 12), dubbed the nuclear ring, of H II regions of radius 2″ (40 pc) surrounding the projection of the compact high-excitation cone. The major axis position angle and axial ratio of the nuclear ring are the same as those of the galaxy disk, so the ring is an intrinsically circular structure in the disk plane. Some of the [Fe II] $\lambda 1.644$ μm emission coincides with this ring and is thus presumably emitted by supernova remnants. The nature of the more compact [Fe II] emission, close to the nucleus, is less clear.

Our images also show the well-known ring of H II regions of radius 8″–14″ (150–270 pc; Figs. 2, 3, and 4) in unprecedented detail. The apparent major axis of this ring is inclined by $\sim 30°$ from the disk major axis, and it is rounder than the disk isophotes. If coplanar with the galaxy disk, it must be elliptical in shape. Dust bands strongly influence the morphology of this ring, particularly to the south of the nucleus.

3. *The warm molecular hydrogen.*—The H_2 $v = 1$ $S(1)$ image shows emission extending some 1″ (20 pc) from the nucleus (Fig. 11). This emission abuts the south edge of the compact cone of ionized gas, suggesting a continuous gaseous structure of which part is ionized and part molecular. The molecular gas is apparently warmed by the nuclear source to the temperatures needed for H_2 $v = 1$–0 $S(1)$ emission.

4. *Disk starlight.*—As expected, dust bands and reddening are most prominent on the near (southeast) side of the galaxy disk (Figs. 1, 2, 4, 6, 7, and 8). The bluest (in $V-K$) regions of the disk are bluer than found in bulge-dominated galaxies, apparently because of the presence of young stars.

5. *The compact nuclear infrared source.*—Our observations confirm the existence of a compact (<2 pc), very red ($\alpha \simeq 7.0$, $S \propto \nu^{-\alpha}$) continuum source in the K band (Figs. 6 and 8). It is proposed that this source is a Seyfert 1 nucleus obscured by $A_V = 28 \pm 7$ mag of extinction. This extinction is smaller than expected from the X-ray-absorbing column ($N_H = 4 \times 10^{24}$ cm^{-2}) and a normal gas-to-dust ratio, and we have argued that the infrared source is indeed observed through a smaller column of gas than the X-ray source.

This research was supported by STScI and NASA through grants GO7273 and NAG 81027, respectively. C. S. and T. S. B. wish to thank the staff of the Space Telescope Science Institute for their hospitality and especially Christine Ritchie and Roeland van der Marel for useful discussions. We thank Sylvain Veilleux for valuable comments on the manuscript.

REFERENCES

Binette, L., Wilson, A. S., Raga, A., & Storchi-Bergmann, T. 1997, A&A, 327, 909
Blietz, M., Cameron, M., Drapatz, S., Genzel, R., Krabbe, A., van der Werf, P., Sternberg, A., & Ward, M. J. 1994, ApJ, 421, 92
Braatz, J. A., Wilson, A. S., Gezari, D. Y., Varosi, F., & Beichman, C. A. 1993, ApJ, 409, L5
Braatz, J. A., Wilson, A. S., & Henkel, C. 1997, ApJS, 110, 321
Buta, R. 1995, ApJS, 96, 39
Cardelli, J. A., Clayton, G. C., & Mathis, J. S. 1989, ApJ, 345, 245
Cid Fernandes, R., & Terlevich, R. 1995, MNRAS, 272, 423
Colina, L. 1993, ApJ, 411, 565
Curran, S. J., Johansson, L. E. B., Rydbeck, G., & Booth, R. S. 1998, A&A, 338, 863
Davies, R. I., et al. 1998, MNRAS, 293, 189
Dopita, M. A., & Sutherland, R. S. 1995, ApJ, 455, 468
Elmouttie, M., Haynes, R. F., Jones, K. L., Ehle, M., Beck, R., & Wielebinski, R. 1995, MNRAS, 275, L53
Elmouttie, M., Haynes, R. F., Jones, K. L., Sadler, E. M., & Ehle, M. 1998a, MNRAS, 297, 1202
Elmouttie, M., Koribalski, B., Gordon, S., Taylor, K., Houghton, S., Lavezzi, T., Haynes, R., & Jones, K. 1998b, MNRAS, 297, 49
Elmouttie, M., Krause, M., Haynes, R. F., & Jones, K. L. 1998c, MNRAS, 300, 1119
Fadda, D., Giuricin, G., Granato, G. L., & Vecchies, D. 1998, ApJ, 496, 117
Forbes, D. A., & Ward, M. J. 1993, ApJ, 416, 150
Freeman, K. C., Karlsson, B., Lynga, G., Burrell, J. F., van Woerden, H., & Goss, W. M. 1977, A&A, 55, 445
Frogel, J. A. 1998, PASP, 110, 200
Frogel, J. A., Persson, S. E., Aaronson, M., & Matthews, K. 1978, ApJ, 220, 75
Gardner, F. F., & Whiteoak, J. B. 1982, MNRAS, 201, 13P
Genzel, R., et al. 1995, ApJ, 444, 129
Glass, I. S., & Moorwood, A. F. M. 1985, MNRAS, 214, 429
González Delgado, R. M., et al. 1998, ApJ, 505, 174
Greenhill, L. J., Ellingsen, S. P., Norris, R. P., Gough, R. G., Sinclair, M. W., Moran, J. M., & Mushotzky, R. 1997, ApJ, 474, L103
Greenhill, L. J., Herrnstein, J. R., Ellingsen, S. P., Reynolds, J. E., Norris, R. P., Moran, J. M., & Booth, R. S. 1998, BAAS, 30, 1332
Heckman, T. M., et al. 1997, ApJ, 482, 114
Hubble, E. 1943, ApJ, 97, 112
Keel, W. 1991, PASP, 103, 723
Kotilainen, J. K., Ward, M. J., Boisson, C., DePoy, D. L., & Smith, M. G. 1992, MNRAS, 256, 149
Krolik, J. H., & Begelman, M. C. 1988, ApJ, 329, 702
Leitherer, K., & Heckman, T. M. 1995, ApJS, 96, 9
Maiolino, R., Alonso-Herrero, A., Anders, S., Quillen, A., Rieke, M. J., Rieke, G. H., & Tacconi-Garman, L. E. 2000, ApJ, 531, 219
Maiolino, R., Krabbe, A., Thatte, N., & Genzel, R. 1998, ApJ, 493, 650
Marconi, A., Moorwood, A. F. M., Origlia, L., & Oliva, E. 1994, ESO, Messenger, 78, 20

Matt, G., et al. 1996, MNRAS, 281, L69
———. 1999, A&A, 341, L39
McLeod, K. K., & Rieke, G. H. 1995, ApJ, 441, 96
Moorwood, A. F. M., & Glass, I. S. 1984, A&A, 135, 281
Moorwood, A. F. M., Lutz, D., Oliva, E., Marconi, A., Netzer, H., Genzel, R., Sturm, E., & de Graauw, T. 1996, A&A, 315, L109
Nussbaumer, H., & Storey, P. J. 1988, A&A, 193, 327
Oliva, E., Marconi, A., Cimatti, A., & di Serego Alighieri, S. 1998, A&A, 329, L21
Oliva, E., Marconi, A., & Moorwood, A. F. M. 1999, A&A, 342, 87
Oliva, E., Salvati, M., Moorwood, A. F. M., & Marconi, A. 1994, A&A, 288, 457
Rieke, G. H., & Lebofsky, M. J. 1985, ApJ, 288, 618
Simcoe, R., McLeod, K. K., Schachter, J., & Elvis, M. 1997, ApJ, 489, 615
Simpson, C. 1998, ApJ, 509, 653
Simpson, C., Forbes, D. A., Baker, A. C., & Ward, M. J. 1996, MNRAS, 283, 777
Storchi-Bergmann, T., Rodriguez-Ardila, A., Schmitt, H. R., Wilson, A. S., & Baldwin, J. A. 1996, ApJ, 472, 83
Storchi-Bergmann, T., Winge, C., Ward, M. J., & Wilson, A. S. 1999, MNRAS, 304, 35
Veilleux, S., & Bland-Hawthorn, J. 1997, ApJ, 479, L105
Weinberger, A. J., Neugebauer, G., & Matthews, K. 1999, AJ, 117, 2748
Wilson, A. S. 1992, in Physics of Active Galactic Nuclei, ed. S. J. Wagner & W. J. Duschl (New York: Springer), 307
Wilson, A. S., Braatz, J. A., Heckman, T. M., Krolik, J. H., & Miley, G. K. 1993, ApJ, 419, L61